

Recyclability of additively manufactured bio-based composites

Katie Copenhaver^{a,*}, Tyler Smith^a, Kristina Armstrong^a, Dipti Kamath^a, Mitchell Rencheck^a, Samarthya Bhagia^b, Matthew Korey^a, Meghan Lamm^a, Soydan Ozcan^a

^a Manufacturing Science Division, Oak Ridge National Laboratory, Oak Ridge, TN, 37830, USA

^b Biosciences Division, Oak Ridge National Laboratory, Oak Ridge, TN, 37830, USA



ARTICLE INFO

Handling Editor: Dr Hao Wang

ABSTRACT

As the flexibility, efficiency, and application space of additive manufacturing continues to grow, many have begun to investigate more sustainable feedstocks as well as options for the end of life of additively manufactured parts. This study examines the effects of mechanical recycling on additively manufactured parts from bio-based feedstock. Articles were printed on the Big Area Additive Manufacturing (BAAM) system at the Oak Ridge National Laboratory using poly (lactic acid)/wood flour (PLA/WF) pellets. These parts were shredded and granulated, and the granulate was fed directly back into the BAAM system for re-printing, skipping the costly and energy-intensive steps of extrusion and pelletization. The chemical, mechanical, thermal, and rheological changes to PLA/WF before and after recycling were investigated. Additionally, the energy savings from directly printing granulate on the BAAM system without extrusion and pelletization is reported. It is shown that PLA/WF is an excellent candidate for recycling of large format additively manufactured parts, and value of these parts can be reclaimed while saving cost and energy through mechanical recycling.

1. Introduction

Interest in additive manufacturing (AM, also known as 3D printing) has exploded in recent years, with constant improvements from emerging robotics and machinery, process control and simulation, and feedstocks. Fused deposition modeling (FDM) of thermoplastics is among the most popular 3D printing methods, and commercially available systems can range in size from the desktop scale, $\sim 0.3\text{ m}^3$, to $90+\text{ m}^3$ build volumes [1]. In addition to the complex geometries and high-fidelity parts achievable with AM, it typically produces less waste than traditional manufacturing methods and can enable a distributed manufacturing system in which production occurs at or near the location of the end-user. The distribution of manufacturing could also encourage the use of local materials and resources, improve supply chain stability, enhance local economies, and ultimately enable more sustainable manufacturing practices [2].

Large format additive manufacturing (LFAM) systems such as the Big Area Additive Manufacturing (BAAM) co-developed by Oak Ridge National Laboratory (ORNL) and Cincinnati, Inc., have opened a variety of new application spaces for AM in areas such as large-scale tooling, aerospace, building and construction, marine, and wind energy [3]. These systems are often pellet-fed and can be used to print neat polymers

as well as fiber-reinforced thermoplastic composites. Typical feedstocks for LFAM systems include engineering plastic resins such as acrylonitrile butadiene styrene (ABS), polyethylene terephthalate glycol (PETg), poly (lactic acid) (PLA), and such high-performance polymers as polyether ether ketone (PEEK) and polyetherimide (PEI), which are often reinforced with carbon or glass fibers [4]. Of those feedstocks, ABS and PLA are the most commonly used for both small and large scale printers [5].

With the increasing attention on sustainability and the effects of industrial processes and waste on the environment, plastic waste and pollution has become a subject of particular scrutiny. Research interest has accordingly risen in the development of bio-based alternatives to petroleum-derived plastics as well as biodegradation and recycling of plastics [6]. As mentioned, PLA is a popular material used in AM and is currently one of the only completely bio-based polymers available for AM feedstocks on a commercial scale [7]. To enhance the properties and lower the cost of PLA while maintaining its sustainable and bio-based qualities, natural particles or fibers such as wood flour (WF), bamboo, flax, and hemp fibers are often added as reinforcing agents [8–11]. Wood-plastic composites in particular have been used widely as long-lasting and sustainable alternatives to timber products for construction materials such as decking, cladding, and framing [12]. Using these sustainable materials as feedstocks for LFAM can further reduce its

* Corresponding author.

E-mail address: copenhaverke@ornl.gov (K. Copenhaver).

carbon footprint and expand the potential applications for bio-based plastics and composites. Fiber-reinforced composite LFAM feedstocks have found notable success in the production of tooling, and bio-based composites such as PLA/WF are excellent candidates to produce low temperature molds. The potential to recycle and re-print such materials for new tooling could further lower their cost and environmental impact [13]. This study explores the potential to recycle bio-based LFAM parts to determine if recycled feedstock could be used again and retain its value in the same application.

A typical mechanical recycling process for thermoplastic polymers and composites consists of shredding or grinding and re-extrusion into a filament, which can be further cut to pellets [14,15]. Numerous studies have been conducted on the recycling of thermoplastic composites, including PLA-based composites and small-scale AM parts, but very few studies are available on either the recycling of LFAM parts or on the ability of printers to process nonuniformly-sized feedstock [10,14, 16–20]. As the BAAM system was designed to accommodate pellets of varying shapes and sizes, this study explored printing articles directly from recycled granulate, skipping the costly and time-consuming extrusion and pelletization steps that can also degrade fibers and polymer matrices [10]. The material properties of samples printed from virgin feedstock and recycled granulate on the BAAM system were characterized and compared, and the energy savings of mechanical recycling without extrusion and repelletization was calculated.

2. Materials and methods

2.1. Materials

2.1.1. PLA/WF

Poly(l-lactide), herein referred to as PLA (Ingeo 4043D, NatureWorks, LLC), compounded with 20 wt% of WF (100 mesh softwood pine) was purchased from Techmer PM, LLC (HiFill PLA 1910 3DP) in the form of pellets 3 mm in diameter and 2 mm in length.

2.2. Sample production

2.2.1. BAAM printing

Samples were printed on the Big Area Additive Manufacturing (BAAM) large-scale thermoplastic extruder. The BAAM consists of a single screw extruder mounted on a gantry system above a heated bed. An image of the BAAM extruder and gantry is available in the supporting information (SI, Fig. S1). PLA/WF pellets or recycled granulate (described below) were placed in a forced-air dryer (Dri-Air Industries, Inc.) held at approximately 60 °C for 4 h prior to printing. Dry pellets/granulate were continuously fed from the dryer to the extruder during printing using a vacuum system. A polycarbonate build sheet was placed on the bed heated to 60 °C and held in place with a separate vacuum system. The BAAM extruder consists of five heating zones which were set to a profile of 170-190-210-215-200 °C, with the lowest temperature at the pellet feeding zone (top) and highest temperatures at the nozzle (bottom). The temperature profile was chosen to aid in extrusion of the materials and minimize the load on the extruder motor while avoiding thermal degradation of the feedstocks. The BAAM was fitted with a 7.6-mm diameter nozzle, which is a standard nozzle size produced by Cincinnati, Inc. for the system.

Hexagonal samples 254 mm on each wall and 229 mm in height were printed using virgin PLA/WF pellets and recycled granulate and identical processing parameters. For each print, the screw speed was set to 83 RPM, and the gantry speed was set to 31.75 mm/s. The screw speed and gantry speed are coupled in the BAAM operating system to maintain a constant bead geometry. The combination of screw speed, gantry speed, and nozzle size used in this study resulted in beads with a height of 3.8 mm and width of 8.6 mm. The layer time for each layer was approximately 2 min and 40 s, and each hexagon consisted of 60 layers of single-bead walls. Two hexagons were produced per print to provide an

adequate layer time for cooling and avoid wall instability, and extra samples using virgin PLA/WF were printed to generate recycled feedstock. Various LFAM systems will differ depending on the manufacturer and model of the equipment, but care must be taken in selecting nozzle sizes, screw speeds, and gantry speeds, among other variables, to extrude consistent beads at a rate the extruder motor can sustain while optimizing the layer times to produce quality parts free of warpage or cracking. Considerations in selecting LFAM parameters and the effects of the numerous variables in printing on the BAAM system have been previously documented [21,22].

2.2.2. Waterjet cutting and shredding/granulating

The additional hexagonal samples printed with virgin PLA/WF were cut first to individual walls and subsequently to approximately 25 × 25 × 25 mm³ cubes using a waterjet cutter (Wardjet X-1530). The cubes were then fed into a desktop shredder/granulator (3devo SHR3D IT) with a 3 mm screen. Granulated material was collected and used directly as feedstock for printing on the BAAM system and injection molding.

2.2.3. Injection molding

Dogbone samples (ASTM D638 Type I) for tensile testing were produced in a 35-ton injection molding (IM) machine (BOY 35 E VV) using virgin PLA/WF pellets and recycled PLA/WF granulate. Prior to IM, the PLA/WF pellets and granulates were dried in an oven (Thermo Fisher Scientific Heratherm Oven) at 60 °C overnight. The five heating zones of the injection molder were set to a temperature profile of 171-182-193-193-193 °C, and PLA/WF pellets or granulate were plasticized at a rate of 300 mm/s to create a 30 mm shot. The temperature profile in the IM machine was selected to be similar to that used on the BAAM but was kept slightly lower than those used during printing. The IM machine can operate at a much higher pressure than the BAAM extruder, meaning it can process material at a higher viscosity. Shots of material were injected into the dogbone mold using a pressure of 17 MPa. The mold is designed such that all material for each sample enters at one end and flows along the length of the dogbone. Images of the IM machine and dogbone mold are shown in the SI (Figs. S2–3). The dogbone mold is connected to a circulating chiller which maintains its temperature at 21 °C. After injection molding, dogbones were held in the mold for approximately 30 s to allow the material to cool below its glass transition temperature (T_g) before being ejected. This process was repeated for both the PLA/WF pellets and granulate.

2.3. Characterization

2.3.1. Tensile testing

Printed hexagonal samples were machined to dogbone (ASTM D638 Type I) specimens for tensile testing. Samples were taken from the midpoint of the walls, centered around layer 30. Samples were taken from both the direction parallel (“x-direction”) and perpendicular (“z-direction”) to the printing path. The dogbone specimens were tested for tensile strength and modulus utilizing an MTS 312.21 mechanical testing frame equipped with a 2500 lbf load cell. Each sample was tested at a rate of 5 mm/min and a 1-inch extensometer (Epsilon) was employed to determine the strain. A minimum of five specimens were tested for each sample type.

2.3.2. Microscopy

The fracture surfaces of virgin and recycled, printed and IM samples after tensile testing were sputtered with iridium and imaged using a scanning electron microscope (SEM, Zeiss Merlin field emission) in secondary electron mode at an accelerating voltage of 1 kV. Unprocessed WF was also sputtered with iridium and imaged using SEM. Tensile sample fracture surfaces were also imaged using a digital optical microscope (Keyence VHX-700F).

2.3.3. Gel permeation chromatography (GPC)

GPC was performed on virgin PLA/WF pellets and recycled granulate according to ASTM D3536 to determine the effect of recycling on the molecular weight of the feedstock. Samples were cut into small pieces and placed into scintillation vials with tetrahydrofuran (THF) overnight with magnetic stirring and then syringe filtered. GPC was carried out on Agilent 1200 SEC system with Waters Styragel 5E, Styragel 3, and Styragel 0.5 columns with 0.5 mL/min THF mobile phase and calibration was based on polystyrene standards. Measurements were conducted twice for each sample type.

2.3.4. Rheology

Samples for rheological analyses were prepared by compression molding virgin PLA/WF pellets and PLA/WF granulate. The feedstocks were first dried overnight at 60 °C, after which the pellets and granulate were placed in a disk-shaped mold 25 mm in diameter and 1.5 mm in thickness. The mold and materials were placed between two steel plates and loaded into a hydraulic press (Carver 3693) with upper and lower platens heated to 180 °C.

Rheological analyses were conducted using a strain-controlled rotational rheometer (ARES-G2, TA Instruments) with 25 mm aluminum parallel plates at a gap of 1 mm. Oscillatory strain sweeps were first performed on virgin and recycled samples to identify their linear viscoelastic regions (LVR). Strain sweeps were performed at 180 °C from 0.01 to 100% strain at an angular frequency of 3 Hz. Frequency sweeps were then conducted on each sample at a strain amplitude in its LVR at 180 °C. The storage and loss moduli and complex viscosity of the samples were recorded at a frequency range of 0.05–200 rad/s. Measurements were conducted twice for each sample type.

Forward and reverse transient stress growth experiments were also performed on virgin and recycled samples at 180 °C in the same configuration used for oscillatory measurements. Samples were sheared for 180 s at a rate of 0.1 s⁻¹ (“forward shear”), after which they were allowed to rest for 1, 60, or 180 s. The samples were again sheared for 180 s at a rate of -0.1 s⁻¹ (“reverse shear”). A new sample was used for each experiment with varying dwell times, totaling 6 measurements. The resulting stress in each sample was recorded as a function of strain.

2.3.5. Dynamic mechanical analyses (DMA)

DMA (TA Instruments DMA 850) was performed on virgin and recycled PLA/WF rectangular (64 × 10 × 3 mm) samples machined from printed hexagons. Samples were machined and tested in directions parallel (“x-direction”) and perpendicular (“z-direction”) to the printing path according to ASTM D5418. Samples were clamped with a dual cantilever clamp, and temperature sweeps were performed at a constant frequency of 1 Hz and amplitude of 15 µm. Each sample was heated during testing from 30 to 120 °C at 3 °C/min. Measurements were conducted twice for each sample type.

2.3.6. Differential scanning calorimetry (DSC)

DSC measurements were performed on a TA instruments Q2000 according to ASTM D3417 using approximately 5 mg of material in sealed aluminum pans. Samples were first equilibrated at 35 °C, after which they were heated from room temperature to 200 °C at 10 °C/min. Sample were then cooled to 35 °C at 10 °C/min and subsequently heated again to 200 °C at 10 °C/min. The degree of crystallinity of each sample was calculated using equation (1):

$$X_c = \frac{\Delta H_m - \Delta H_c}{\Delta H_f^0 \cdot \varphi} \quad (1)$$

in which ΔH_m and ΔH_c denote the melting and cold crystallization enthalpies, respectively, of each sample, ΔH_f^0 denotes the melting enthalpy of a 100% crystalline PLA sample, and φ denotes the mass fraction of PLA in each sample. The value of ΔH_f^0 for PLA was taken as 93 J/g, and φ was equal to 0.8 for all samples in this study [23].

The melting and cold crystallization enthalpies from the second heating scan were used to calculate the crystallinities of the virgin pellets and granulate to remove the effect of prior processing on the samples’ structure. The enthalpies from the first heating scan were used to calculate the crystallinities of all printed and IM samples, however, to note the effect of the different processing methods on the materials. Measurements were conducted twice for each feedstock material and four times for each AM and IM sample due to sample variability.

2.4. Energy analysis

The relative embodied energies of the injection molded virgin material and the injection molded recycled granulate were calculated using a bottom-up approach. Experimental data for recycling process energies were collected from a large-scale shredder and granulator at ORNL (MR40120 shredder and 56U granulator, Cumberland Plastics, Inc.), to estimate the embodied energy at a pilot-scale. This pilot-scale system can process composite parts up to 1.8 m³; as such, the energy consumption of waterjet cutting was not included in the estimation of pilot-scale recycling. The specific energy use for the large-scale shredder/granulator was estimated from recycling trials using several batches of ABS/carbon fiber composite materials, and the starting weight, run times, and current draws of each batch were recorded. Additional data for the embodied energy of the virgin materials were obtained from literature. The embodied energy for PLA was obtained from EcoInvent [24], whereas WF was considered a by-product from softwood pulping and assumed to have no embodied energy. The PLA/WF material was assumed to be successively recycled up to four times. The embodied energy values of the virgin and recycled materials were estimated over four recycling cycles, or five product life cycles.

3. Material processing and characterization results

3.1. Additive manufacturing and sample preparation

Additive manufacturing with PLA and PLA-based composites has been demonstrated widely from a desktop to industrial scale. WF is a common additive to PLA, as it is a widely available and inexpensive waste material that can significantly reduce the cost of AM feedstocks while improving the printability of the material and the mechanical performance and structural integrity of printed parts [1]. Furthermore, using recycled materials as AM feedstock and the effect of recycling on natural fiber-reinforced composites has been well-studied [10]. However, direct re-printing of shredded and granulated material has not yet been demonstrated on a large scale. The recycling and potential re-use of bio-based LFAM composite parts was demonstrated in this study by printing test pieces that were then shredded, granulated, and re-printed.

Material printed with virgin PLA/WF pellets after cutting, shredding, and granulating is shown in Fig. 1. The granulate was produced using a 3-mm screen, but the resulting particles are clearly inhomogeneous in size. For this reason, recycled feedstock for AM or IM is typically re-extruded and pelletized to produce uniform recycled pellets [14]. However, this study aimed not only to ascertain the effects of reprocessing on the structure and performance of the material, but also to determine if the pelletization step could be avoided altogether, eliminating a costly step that could also cause deterioration and property loss of the composite. Here, PLA/WF granulate was fed directly back into the BAAM system and injection molder without further processing or sieving. Very large or inhomogeneous particles often clog or have issues feeding in extrusion-based AM systems, which tend to stem from pellet bridging along the feed tube or in the entrance of the screw, preventing material flow. However, the PLA/WF granulate, containing particles ranging from 4+ mm to small, dust-like pieces, presented no issues in feeding from the dryers to the hopper and extruder of the BAAM [19,25]. It has been demonstrated previously that careful design of the feed throat and temperature control of the upper heating zones of the

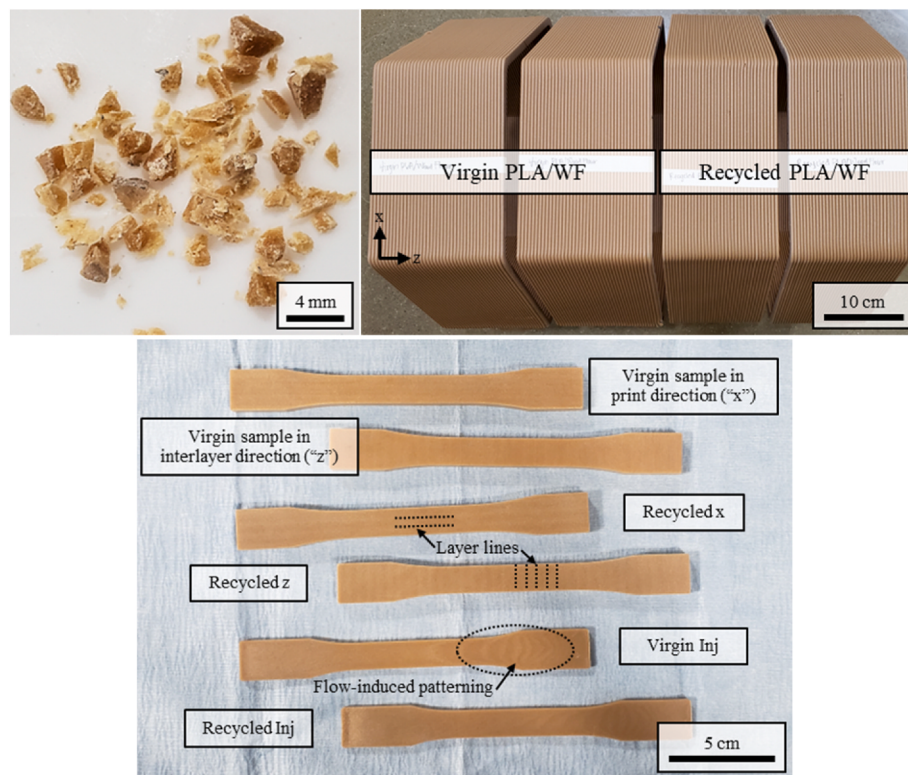


Fig. 1. PLA/WF granulate showing inhomogeneity in particle size (top left), hexagons printed on BAAM from virgin and recycled PLA/WF (top right), and virgin and recycled AM and IM samples (bottom). Dotted lines and circles on AM and IM samples indicate printed layers in AM samples and flow path of material in IM samples, respectively.

extruder on the BAAM can eliminate pellet bridging and allow for steady, continuous feeding with pellets of various sizes [26]. The successful printing of granulate in this study proves that particles of various shapes and sizes can be extruded using the BAAM system.

Virgin and recycled hexagonal samples printed on the BAAM system are shown in Fig. 1 along with their corresponding machined tensile samples and IM tensile samples. The virgin and recycled prints were virtually indistinguishable from one another, indicating there was little degradation of the polymer matrix or filler after recycling, which could have resulted in discoloration. The machined AM and IM samples also displayed unique identifying features. Horizontal and vertical striations are faintly visible on the printed samples taken in the direction of printing ("x") and in the interlayer direction ("z"), respectively, that correspond to the different printed layers. A similar multi-tonal effect can be seen on the IM samples, which is most likely a result of the flow path of the polymer melt as it is injected into the mold at ambient

temperature. These features are marked with dotted lines in Fig. 1.

3.2. Tensile testing

The AM and IM virgin and recycled PLA/WF dogbone samples were then subjected to tensile testing to determine their strengths, elastic moduli, and strains at failure, and results are shown in Fig. 2. The stress-strain curves from which these values were calculated are shown in the SI (Fig. S4).

Regardless of processing method, the addition of WF to PLA typically decreases its tensile strength and strain to failure while increasing its tensile modulus, with neat IM PLA possessing a tensile strength, modulus, and failure strain of approximately 60 MPa, 3.6 GPa, and 6%, respectively [27]. The reduction in strength and failure strain is likely attributable to ineffective stress transfer from the PLA matrix to the WF particles due to their lack of compatibility at their interface as well as the

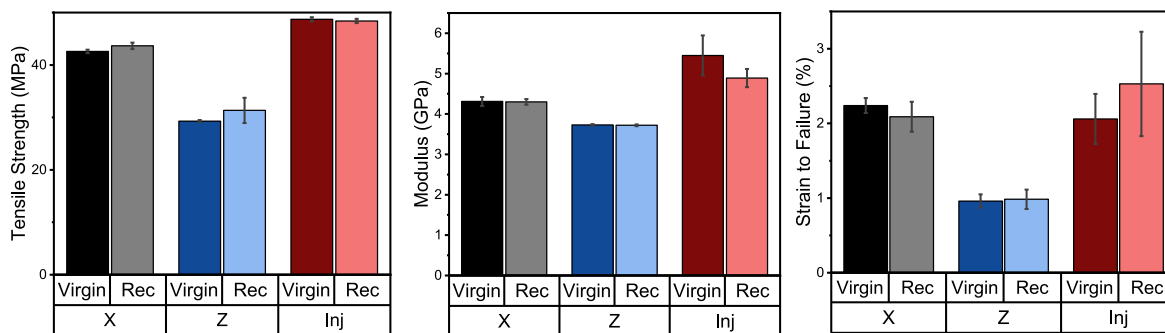


Fig. 2. Tensile strength (left), modulus (center), and strain to failure (right) of AM and IM, virgin and recycled PLA/WF samples. "X" refers to printed samples taken in the printing direction, "Z" refers to printed samples taken in the interlayer direction, "Rec" refers to material printed or molded with the recycled granulate, and "Inj" refers to injection molded samples.

inhomogeneity and low aspect ratio of the WF. For the AM parts, the strengths, moduli, and failure strains tend to be higher along the print direction than along the perpendicular, interlayer direction. This mechanical anisotropy is well-known and documented in literature [4,22, 28–35]. The reduction in mechanical performance in the z-direction is a result of the temperature gradient between the previously deposited layer and the melt being deposited. Interlayer bonding relies on polymer diffusion, which in turn depends on the mobility of polymer chains in adjacent layers and their contact area [28]. Shorter layer times (i.e., faster printing) can reduce this temperature gradient, but excessive heat retention can lead to instability, sagging, or failure of a part during printing. The mechanical properties in the x-direction of a print also benefit from orientation of polymer chains and any fibers present in a composite matrix during extrusion. The high degree of shear administered to the composite leads to polymer chain and fiber orientation along the print direction and further minimizes polymer diffusion and chain entanglement between layer, and as a result, the z-direction of a printed composite part cannot benefit from the strength or high aspect ratio of reinforcing fibers [29].

The tensile strength of AM parts has been reported to drop by 30–60% between the x- and z-directions in PLA-based parts [30]. The mechanical properties shown in Fig. 2 fall within this range, with a 30% loss in strength between x- and z-direction virgin samples (42.5–29.3 MPa, respectively) and a 28% loss in strength between x- and z-direction recycled samples (43.7–31.3 MPa, respectively). The difference in strain to failure between the x- and z-direction samples was even more severe, with a 57% reduction in failure strain between x- and z-direction virgin samples (2.24%–0.96%, respectively) and a 53% reduction in failure strain between x- and z-direction recycled samples (2.09%–0.98%, respectively). Notably, the x-direction samples (both virgin and recycled) exhibited plastic deformation before failure, while the z-direction samples exhibited purely brittle failure (SI, Fig. S4). Both the virgin and recycled samples exhibited identical moduli in each respective direction and a 14% decrease comparing the x- and z-directions (4.3–3.7 GPa, respectively). Furthermore, the tensile strength and modulus of the printed PLA/WF composites are similar to other PLA/WF composites reported in literature [1,8,36,37].

The mechanical properties of polymers and composites often suffer after mechanical recycling, attributable to polymer degradation due to chain scission, changes in crystallinity, fiber breakage, and/or degradation of the matrix/filler interface [10]. The PLA/WF materials used in this study, however, showed little to no change in mechanical performance after thermomechanical recycling. A nearly constant maintenance of a composite's mechanical performance after thermomechanical recycling might suggest that there were no changes within the material during reprocessing; however, it is likely that a combination of ultimately neutralizing factors are responsible for the lack of change in properties [10]. Repeated thermomechanical processing often causes some loss in molecular weight of a polymer, particularly in PLA, which is highly susceptible to hydrolytic degradation at high temperatures [38]. The presence of natural fibers or fillers can also exacerbate the degradation of PLA as a result of the hygroscopic nature of natural fibers and the increased shear caused by the fibers during processing [10,39–41]. Thermomechanical recycling can also improve some aspects of composites that contribute to their mechanical performance. For example, a better dispersion of fiber or filler within a matrix can be obtained after multiple processing steps. Additionally, the WF particles can break up during processing, as WF consists of bundles of wood fibers. This could lead to more numerous, smaller particles with potentially higher aspect ratios, each of which could improve the composite's mechanical performance [42].

Finally, the virgin and recycled IM samples yielded a higher tensile strength and modulus than any of the printed samples with similar strains to failure as the x-direction AM samples. AM often leads to voids within a material, both in between layers and within the deposited beads themselves [8,43]. Intra-bead voids or porosity has also been shown to

be more prevalent in printed parts when fibers or particles are added to the matrix [44,45]. The presence of voids generally causes AM parts to be less dense than compression- or injection-molded counterparts, which results in a reduced mechanical performance as the voids serve as regions of stress concentration from which cracks can more easily initiate under loading. Furthermore, the strain at which a material fails in tension is highly sensitive to defects within the material [8,43,44,46]. The AM samples showed consistent strains to failure in comparison with that of the IM samples. As stated, potential voids or porosity in the AM samples are likely responsible for crack initiation and ultimate failure. A lower porosity in the IM samples could mean that failure was more dependent on the WF itself. Heterogeneity of the WF in shape and size could be responsible for the large variations seen in the failure strains of the IM samples in Fig. 2. Finally, the degree of fiber alignment within a sample can cause a significant difference in its mechanical performance. The IM process is more likely to cause a higher degree of fiber alignment through the high shear and elongational flow within a mold [47]. The effect of changing WF size or content was not studied in this work but would undoubtedly impact the mechanical performance of the virgin composite and its behavior after recycling. The morphology and alignment of the WF and the presence of voids in the composites was then explored with microscopy.

3.3. Microscopy

The WF used in the composites in this study was first analyzed via SEM. The WF purchased was classified as 100 mesh, meaning it was sieved through a screen with 149 μm -sized openings. The WF, shown in Fig. 3, is clearly inhomogeneous, with particles present over a range of aspect ratios. Some particles with dimensions larger than 149 μm are present in the sample, as higher aspect ratio particles could pass through the sieve if rotated in such a way that their smallest dimension fit through the sieve openings.

The fracture surfaces of virgin and recycled AM samples in the x- and z-directions as well as virgin and recycled IM samples were then analyzed using optical microscopy and SEM, shown in Fig. 4.

All images of the AM samples, both optical and SEM, shown in Fig. 4 appear similar, with no obvious differences between the virgin and recycled or x- and z-directions. However, the fractures surfaces of the IM samples are markedly different than the printed samples. The most distinct feature present on all printed sample fracture surfaces is the presence of voids, some of which are indicated with black arrows in Fig. 4. Such voids were seemingly absent from the IM samples, which supports trends reported in literature comparing IM and AM parts [8,37, 43,46]. The voids in the printed samples likely contributed significantly to their reduced mechanical performance in comparison to the IM samples. The void content of all 4 a.m. samples appears similar. The presence of these intra-bead voids is common in AM parts and likely results from air entrapment during feeding and initial melting and

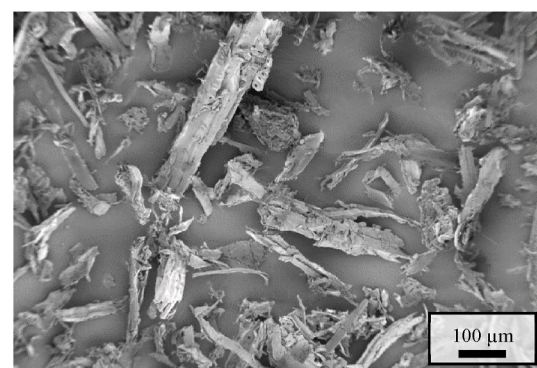


Fig. 3. SEM micrograph of 100 mesh WF illustrating heterogeneity in particle size and aspect ratio.

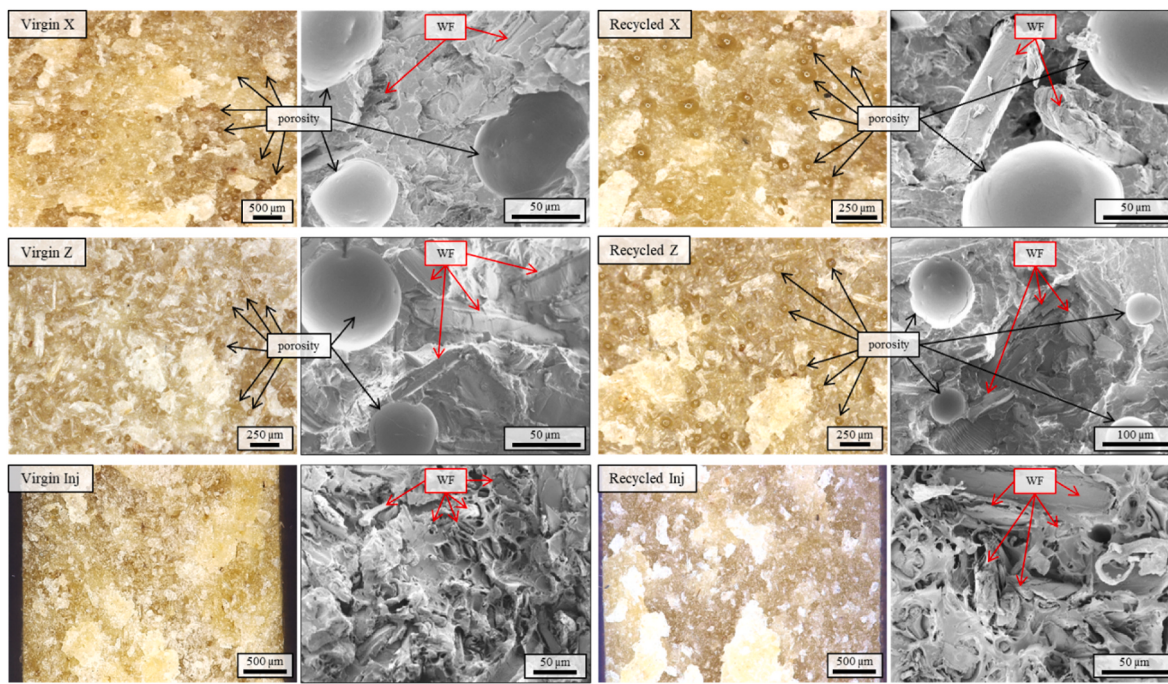


Fig. 4. Optical and SEM images of PLA/WF fracture surfaces from virgin and recycled AM and IM samples. Black arrows on AM sample images indicate large pores, red arrows indicate WF particles.

potential offgassing of the materials during extrusion. Additionally, gaps between fillers and the polymer matrix of composites due to poor interfacial interactions and variations in the coefficient of thermal expansion of the two phases can increase the overall porosity of both AM and IM samples [45,48]. Another key difference contributing to the higher porosity of AM samples in comparison to IM is that material is subjected to high pressure and shear in AM while moving through the screw barrel and nozzle. When material exits the nozzle, it is released to atmospheric pressure, allowing it to expand before cooling. Conversely during IM, material is injected into a mold at a high pressure, and the material is cooled below its T_g before the pressure is released, resulting in a denser structure with lower porosity. Numerous attempts have been made by researchers to reduce porosity and increase the performance of AM parts through techniques such as venting the extruder during printing and using smaller nozzles or screw designs with higher compression ratios [49,50]. The optimization of printing parameters and extruder design for production of PLA/WF parts with minimized porosity bears further investigation. As the virgin and recycled materials were produced with the same extruder configuration and parameters in this study, it can be assumed from analysis of optical and SEM images coupled with the results of tensile testing previously presented that recycling an additively manufactured PLA/WF part has little to no effect on the overall void content after remanufacturing.

Fig. 4 also indicates there is little to no alignment of the WF particles in the printed samples. If properly aligned along the direction of processing (x-direction), particles should appear out-of-plane at the fracture surface, or holes would be visible to indicate pull-out of the particles in the SEM images. Some alignment of the WF particles may be present in the IM samples, as more of the particles appear out-of-plane. This possible alignment would have further contributed to the higher mechanical performance of the IM samples. The degree of shear stress exerted by the injection molder is seemingly higher than that in the BAAM system and could induce some alignment of the heterogeneous and low-aspect ratio WF particles within a PLA matrix. The potential alignment of WF particles in virgin and recycled feedstocks was also investigated through transient stress growth experiments conducted on a rheometer, discussed in a later section.

When comparing the virgin and recycled fracture surfaces of each sample type, there are no obvious differences. The WF particles can be difficult to resolve from the PLA matrix, but there is no clear difference in size or dispersion between the virgin and recycled samples. However, the heterogeneity of the WF particles makes these factors difficult to quantify. A lack of adhesion between the PLA and WF particle surfaces was also observed in the tensile specimens (Fig. 5). Gaps were noticeable between the polymer matrix and WF, which suggests an inability of the polymer to transfer stress to the particles during tensile testing, reducing mechanical performance. The hydrophilic, polar nature of WF renders it incompatible with the hydrophobic, nonpolar PLA matrix. Extensive research has been conducted to optimize the interface between PLA and natural fibers using surface treatments and coupling agents [9,51–53]. These strategies could be applied to the PLA/WF system used in this study, and the performance of such compatibilized composites in AM parts before and after recycling is an avenue for future study.

3.4. Molecular weight measurements

The molecular weights of the virgin pellets and recycled granulate were measured by GPC to assess the extent of degradation of the PLA matrix after mechanical recycling. The weight- and number-average molecular weights (M_w and M_n , respectively) and the dispersity indices (D , defined as the ratio of M_w to M_n) of the virgin and recycled feedstocks are given in Table 1.

The samples exhibited moderate reductions in molecular weight after printing and recycling, with an approximately 18% decrease in M_w and 24% decrease in M_n . Furthermore, the dispersity increased by 7.8%, meaning the distribution of the molecular weights of polymer chains in the samples broadened after recycling. As mentioned previously, a reduction in the molecular weight of a polymer after thermomechanical processing is attributable to chain scission, and PLA is particularly sensitive to hydrolytic degradation at high temperatures such as those used during printing. The presence of any moisture due to inadequate drying or the hygroscopicity of the WF would have exacerbated the molecular degradation. The PLA/WF virgin pellets were dried thoroughly before printing; however, the printed part was not dried before

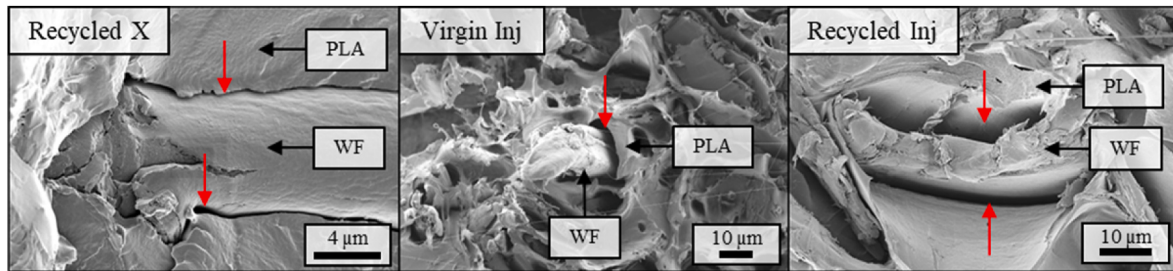


Fig. 5. SEM micrographs of PLA/WF fracture surfaces. Red arrows indicate lack of adhesion at PLA/WF interface.

Table 1

Molecular weight and dispersity of PLA/WF composite samples.

Sample	M_w (kDa)	M_n (kDa)	D
Virgin pellet	167.49 ± 0.29	93.17 ± 0.21	1.80 ± 0.003
Recycled granulate	137.60 ± 0.56	70.80 ± 1.43	1.94 ± 0.02

shredding and granulating. The part undoubtedly absorbed moisture during waterjet cutting, and it is possible high temperatures were generated in the shredder/granulator during recycling. Although the printing step likely heavily contributed to degradation of the PLA matrix, further degradation may have occurred during the subsequent mechanical recycling step. The impact of drying, melt processing, and mechanical recycling on molecular weight is certainly an avenue for further study to conclude the extent of degradation in each processing step. Regardless, the moderate reductions in M_w and M_n and increase in dispersity of PLA after one reprocessing step reflect those documented by numerous researchers in studies of mechanical recycling of PLA [38, 40,54].

3.5. Rheological characterization

The viscoelastic properties of the virgin and recycled feedstocks were then characterized using a parallel plate rotational rheometer to observe the effects of thermomechanical processing and recycling on the material's flow behavior. The storage and loss moduli and complex viscosity were recorded during isothermal frequency sweeps at a constant strain amplitude and are shown in Fig. 6. The recycled samples clearly indicate a lower storage loss/modulus and complex viscosity than the virgin material across the frequency range tested. Differences in the moduli and complex viscosity between the virgin and recycled samples produced from pellets and granulate, respectively, are more evident at low frequencies, which is commonly reported in rheological investigations of thermoplastic composites. The low-frequency region is more indicative of the long-range viscoelastic behavior, in which relatively large fillers such as WF play a larger role [55,56]. Both materials display liquid viscoelastic behavior across most of the range tested, indicated by the storage modulus exceeding the loss modulus. A crossover from loss-dominant to storage-dominant behavior is evident at high frequencies in the virgin PLA/WF plot, while a modulus crossover in the recycled material appears likely to occur at a slightly higher frequency

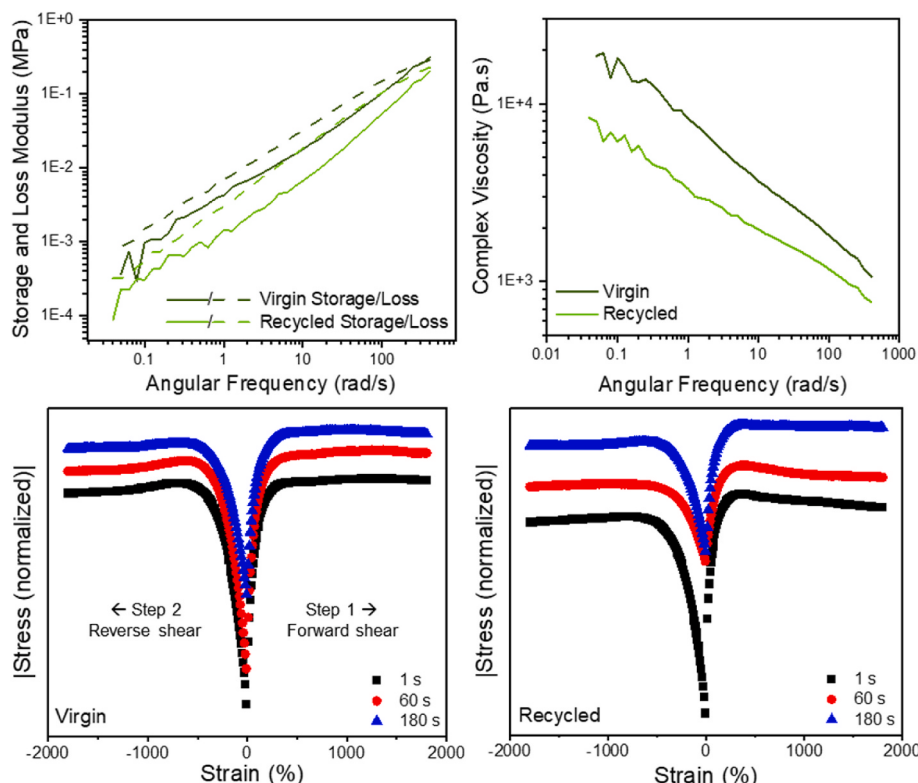


Fig. 6. Rheological analyses of PLA/WF samples compression molded from virgin pellets and recycled granulate. Storage and loss moduli and complex viscosities obtained from oscillatory frequency sweeps are shown at top, and transient stress growth plots in forward and reverse shear are shown on bottom.

than was tested, meaning the material shows a more viscous response over a wider range of frequencies and has a lower characteristic relaxation time. The reduction in storage and loss moduli and the shift in the modulus crossover to higher frequencies between the virgin and recycled samples is likely a consequence of the reduction in molecular weight of the PLA after printing and mechanical recycling.

The complex viscosity of samples made from virgin and recycled PLA/WF reflects the modulus trends in that the complex viscosity was lower across the frequency range tested after recycling. Additionally, the discrepancy between the complex viscosity of the virgin and recycled samples is more evident at low frequencies. The lower complex viscosity of the recycled samples is also likely related to the reduction in molecular weight after reprocessing [57]. Any breakup of the WF particles, which was evidenced by the constant tensile properties before and after recycling despite the decrease in molecular weight, could have contributed to the decrease in complex viscosity, as smaller particles can often flow more easily. Neither of the samples show a measurable trend toward zero-shear viscosity at low frequencies, suggesting the presence of a yield stress attributable to interactions between the micron-sized WF particles. The presence of a yield stress rather than a zero-shear viscosity in oscillatory frequency sweeps is commonly seen in highly filled thermoplastic composites and composites with relatively large fillers [55].

Forward and reverse transient shear flow tests were conducted on the virgin and recycled samples compression molded from pellets and recycled granulate, respectively, with dwell times between the forward and reverse shears ranging from 1 to 180 s to investigate changes in the composite structure and potential alignment of WF particles before and/or after recycling. In thermoplastic composites with high aspect ratio fillers, the application of a shear flow often causes an initial spike in the stress experienced by the system, referred to as a “stress overshoot.” The stress reaches a maximum and then lowers to an equilibrium value as strain is continuously applied. This stress overshoot can be attributed to a rearrangement and alignment of polymer chains and fillers in the

direction of the flow. When the shear flow is halted, the polymer chains and particles can relax, rearrange, and regain entropy, and a resumption or reversal of the shear flow can lead to a second stress overshoot, the magnitude of which can depend on the size of particles, polymer molecular weight, and length of the dwell [55,58]. The virgin and recycled PLA/WF samples were first subjected to a forward shear flow with the applied strain reaching nearly 2000%. Samples were then held for 1, 60, or 180 s, and the strain was reversed, again reaching nearly -2000%, as shown in Fig. 6. The virgin samples exhibited no stress overshoot in forward flow and a very slight overshoot in reverse flow, indicating that some particles within the composite may have aligned with the flow direction. The recycled samples do display very slight stress overshoots when subjected to forward shear and a slight overshoot in the sample allowed to dwell for 180 s before the application of reverse shear, again indicating a small degree of particle alignment. These results again reflect the low aspect ratio and inhomogeneity of the WF particles. In general, the very slight and inconsistent stress overshoots exhibited by each of the samples reflect the very low degree of particle alignment evidenced by the fracture surface analyses detailed above. As such, the differences in tensile strength between the AM and IM samples are more likely attributable to the presence and absence of voids in the respective materials than to differences in WF alignment.

3.6. Thermomechanical characterization

The dynamic mechanical properties of the printed PLA/WF samples in the x- and z-directions were then analyzed using DMA to further investigate the effect of recycling on the anisotropy observed in the mechanical testing results (Fig. 7). In particular, the storage modulus and $\tan \delta$, the ratio of storage and loss moduli, were quantified across a range of temperatures below the material's melting point. The storage modulus reflects the stiffness of a material and is often used to compare the degree of stress transfer from a polymer matrix to fillers or fibers. Additionally, printed composite samples can exhibit anisotropy in their

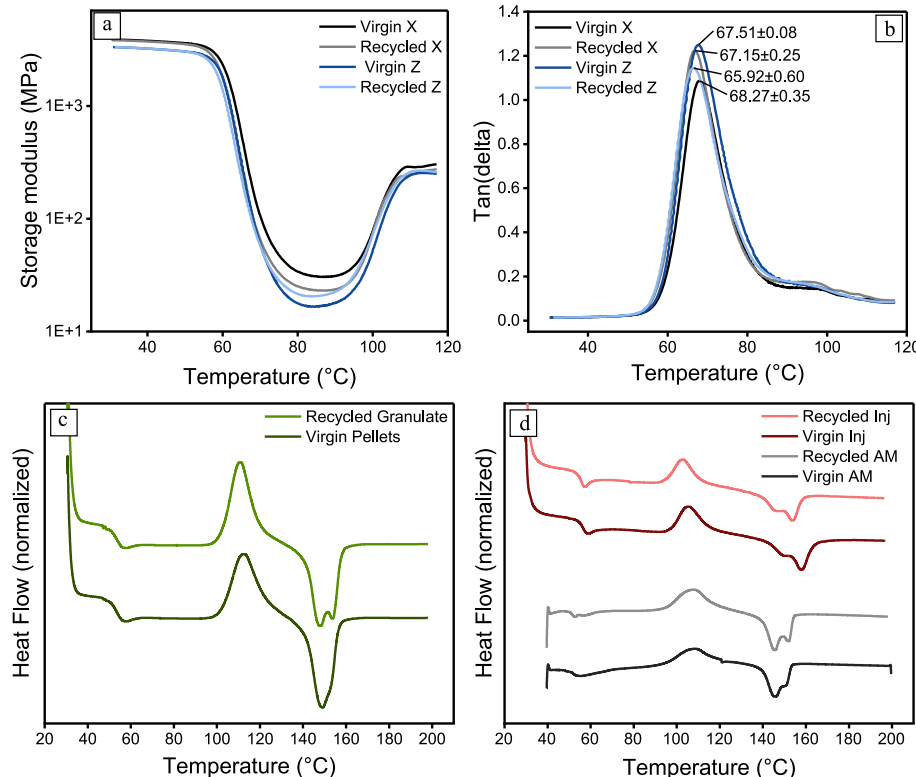


Fig. 7. (a–b) DMA analyses of virgin and recycled AM samples, and DSC analyses of (c) virgin pellets and recycled granulate and (d) virgin and recycled AM and IM samples.

storage moduli depending on whether the sample is oriented parallel to the print direction. Printed composites with highly aligned fillers or fibers can display higher storage moduli in the print direction (x-direction). Unlike tensile testing, anisotropy in the storage modulus measured via DMA is not affected by the weak interface between layers that contributes to reduced tensile performance perpendicular to the print direction [4]. The T_g can also be determined via DMA, and in this study is taken as the peak of the $\tan \delta$ curve, which corresponds to a drop in the storage modulus versus temperature curve, indicating a transition between a glassy and rubbery state [59]. The T_g can be affected by recycling, as degradation of a polymer matrix due to thermomechanical processing can result in shorter, more mobile polymer chains.

As shown in Fig. 7a, there is little difference among the storage modulus curves of the various printed PLA/WF samples. The minimum of the virgin x-direction storage modulus plot is higher than that of the virgin z-direction plot, which could be an indication of some degree of particle alignment. However, the curves of both recycled samples are very similar, and no trend exists in comparison of the virgin versus recycled samples of either direction. The similarity in the storage modulus curves of the printed PLA/WF samples further indicates that alignment of the WF contributes little to the tensile properties of the printed samples, and poor interlayer adhesion is the primary mechanism responsible for the difference in tensile strength and modulus between the x- and z-direction samples.

Representative $\tan \delta$ curves from a single DMA test of the printed virgin and recycled PLA/WF samples in x- and z-directions are shown in Fig. 7b, and the average values and standard deviations of T_g from repeated tests are displayed. The values of T_g are all very similar, although there is a slight decrease from the T_g of the virgin samples in comparison to the recycled samples for both print directions that is outside of the reported error. However, no appreciable difference exists between the x- and z-direction samples of the virgin or recycled sets. The slight decrease in T_g between the virgin and recycled samples can be attributed to the reduction in molecular weight of the PLA, resulting in shorter polymer chains that are more mobile at a slightly lower temperature.

The thermal properties of PLA/WF virgin pellets and granulate produced from recycled AM parts were also investigated using DSC. The second heating curves from these tests, shown in Fig. 7c, were used to compare the virgin and recycled feedstocks with identical thermal histories. The glass transition, cold crystallization onset, and melting onset temperatures of both feedstocks are nearly identical. As discussed previously, polymer degradation due to thermomechanical recycling can cause downward shifts in these temperatures, but these effects are not noticeable in the virgin and recycled PLA/WF feedstocks. However, there is an appearance of a double melting peak after recycling. This has been previously reported by researchers and indicates polymer degradation leading to the formation of less stable crystalline phases that can melt at slightly lower temperatures [10,59]. The cold crystallization and melting enthalpies were then used to calculate the crystallinity of the pellets and granulate, and obtained values are shown in Table 2. The crystallinity of the PLA/WF decreased negligibly upon recycling considering the variability in the experimentally obtained values. An increase in the crystallinity of composites after recycling is usually expected due to the shortening of polymer chains and an increase in the number of fibers or particles [10]. Although a reduction in molecular weight was proven via GPC measurements and enhanced dispersion was indicated by the relatively constant tensile and DMA data before and

after recycling, it is unknown which of these factors contribute the most to this relative lack in the change of crystallization behavior. It is also possible that the reduction in molecular weight led to a reduction in heat capacity of the polymer matrix, which has been reported by other researchers, allowing the polymer to cool faster and hindering crystallization [60,61].

The AM and IM samples were then analyzed via DSC, the results of which are shown in Fig. 7d. The first heating curves are shown, and enthalpies of melting and cold crystallization from the first heating cycles were used to calculate samples' crystallinities. The virgin and recycled AM samples appear very similar, with no distinguishable shift in the T_g or melting and crystallization peaks. In comparing the virgin and recycled IM samples, the thermal transitions of the recycled sample appear to be shifted to slightly lower temperatures. Again, this downward shift in transition temperatures is reflective of the reduction in the molecular weight of PLA after reprocessing. The lack of such a shift in the AM samples could suggest that IM is more damaging to the composite structure than AM, as feedstocks for the recycled AM and IM samples were identical and produced from an AM part. Feedstock recycled from IM parts may exhibit further downward shifts in the temperatures of thermal transitions, which warrants further study but is beyond the scope of this work.

The crystallinity of each AM and IM sample was calculated using information from the first DSC heating curve, and values are listed in Table 2. As described previously, each AM and IM sample was tested 4 times using DSC to obtain average values for the crystalline content of each sample. However, the measurements varied significantly from sample to sample, and the data sets yielded high deviations in comparison to the crystallinity values. The cold crystallization and melting enthalpies as well as measured crystallinities of each sample and the temperatures at onset of cold crystallization and melting are listed in the SI (Table S1). Samples for DSC were taken purposefully from different areas of the IM dogbones and AM parts in attempts to obtain a true average for the bulk of the material. However, the cooling rates can vary throughout a sample or part in both IM and AM. During IM, the molten polymer that first contacts the walls of the cold mold is essentially quenched, forming a "skin" layer with a different morphology than the core of the sample. Material continues to flow past the frozen skin to fill the bulk of the mold, resulting in inhomogeneous properties throughout the part and, in some cases, visible flow patterns such as those shown in Fig. 2. This causes elongation or stretching and alignment of the polymer chains within the mold, facilitating crystallization [62,63]. As a result, IM parts experience a wide range of cooling rates, with the highest at the mold wall and the lowest toward the center of the part. Due to the design of the dogbone mold used to produce IM samples in this study, the crystallinity likely varied along the samples' width and length.

Similarly, the cooling rate of an extruded bead is highest at its outer edge and decreases toward the center of the bead. However, as molten material is extruded with each layer during a print on top of a cooler layer, the previous layer is partially re-melted to fuse with the new layer. In a study of printing ABS filled with 20 wt% carbon fiber on the BAAM system, Compton et al. showed that a layer deposited at 200 °C is rapidly quenched by the underlying layer by up to 30 °C, after which it can cool another 70 °C given a 2-min layer time, resulting in a rapid heat-cool cycle between 200 °C and 110 °C in that time span [64]. The rapid thermal cycling and cooling experienced by the PLA/WF during printing in different regions of the extruded bead and printed part likely contributes to the variation in crystallinity seen among the samples tested by DSC. Ultimately the measured crystallinity of both IM and AM samples was low, with the highest measured value of any sample being 10.76% (virgin IM sample, Table S1). A low crystallinity is desirable in LFAM, as crystallization during cooling can cause shrinkage and exacerbate warpage of the printed part [65]. The lack of increase in the crystallinity of PLA/WF after AM and recycling further demonstrates its viability as a recycled feedstock for AM or IM.

Table 2
Calculated crystallinity of PLA/WF composite samples.

	Virgin	Recycled
Pellets/granulate	0.98 ± 0.002%	0.79 ± 0.44%
AM	5.15 ± 1.78	5.75 ± 1.51
IM	5.04 ± 3.87	3.01 ± 1.28

4. Energy savings

The embodied energy of virgin PLA/WF was assumed to be very similar to that of virgin neat PLA, 71.1 MJ/kg [24]. Any additional energetic contributions from WF were excluded, as mentioned, as it is a waste product. Additionally, the compounding and repelletization of the composite material was assumed to be relatively small and not integrated into the estimate. Other work at ORNL has estimated the energetic cost of extrusion to be less than 0.06 MJ/kg, less than 0.1% of the energy of the neat PLA. The energy required to shred the composite material was determined from experimental data. The shredder and granulator setup has five motors ranging from 7.5 hp to 95 hp. The current from each were monitored over several runs, and the average specific energy use was estimated to be 0.093 MJ/kg, substantially lower than embodied energy of the virgin PLA/WF composite.

This comparative energy demand analysis only considers the energy differences between the embodied and production energies of the to-be-printed materials and not the energies of the manufacturing of the final composites (i.e., printing or injection molding), transportation and use phases, or the final end-of-life, as they are assumed to be identical across the two materials. The embodied energy values of the virgin and recycled materials were estimated for four subsequent recycling cycles or five product life cycles. For each life cycle, the virgin material maintains the same embodied energy; however, the recycled material's embodied energy is the sum of the production energies for each lifetime (virgin material embodied energy at life cycle "1" plus the recycling energy of each subsequent cycle). This is shown in Fig. 8 for the two materials.

With the second lifetime, the embodied energy of the recycled material was slightly higher than half that of the virgin material, as it includes the full energy of the virgin material plus one recycling step, however the recycling stage energy is less than 1% of the material embodied energy, and a nearly negligible contribution to the total lifetime energy. As the recycled material has more lifetimes in use, the reductions in energy demand between life cycles decreases (50% between the first two lifetimes, 17% between the second and third, down to 5% between the fourth and fifth). Therefore, if material degradation does become a problem with more recycling cycles, it may not be energetically beneficial to continue recycling.

5. Conclusions

Recycling and re-use of AM parts made from commercially available bio-based composite feedstock was demonstrated in this study on a large scale with little to no loss in mechanical performance and a substantial energy reduction. This study proved that inhomogeneous composite granulate could be successfully printed on the BAAM system without the need for re-extrusion and pelletization, eliminating an expensive process step that can damage polymer matrices and fibers. It was demonstrated through LFAM and subsequent characterization that the value of additively manufactured parts from PLA/WF feedstock can be reclaimed through simple mechanical recycling, as the tensile and dynamic mechanical properties of the material remained relatively constant and the thermal and rheological properties of the recycled material allowed it to be processed at the same conditions as virgin feedstock. Additionally, the comparison of AM to IM parts highlighted differences in fiber alignment, porosity, and performance imparted by the different manufacturing processes. Finally, the energy analysis confirmed that recycling drastically decreases the embodied energy of PLA/WF parts for each lifetime that the material retains sufficient properties for reuse. As the use of LFAM for rapid prototyping and tooling has become more prevalent, inexpensive and sustainable feedstock such as PLA/WF will likely rise in popularity. This study has shown that not only can PLA/WF be printed successfully on a large format system, but printed parts can be shredded after use and re-printed or injection molded into a new part.

Ultimately, the conservation of mechanical performance of the printed PLA/WF part after recycling was likely a balance between a

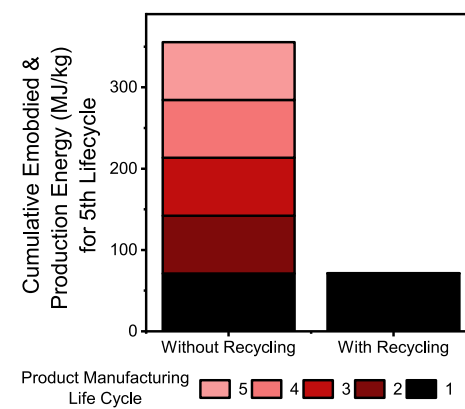


Fig. 8. Life cycle average embodied and production energy of injection molded virgin and recycled materials for five product life cycles, with 1 denoting the initial life where no recycling has occurred. (The energetic contributions of the recycling process (~0.09 MJ/kg per cycle) are too small to be seen in the recycled material plot at this scale.).

reduction in molecular weight of PLA, which weakened the material, and an enhanced dispersion or breakup of the WF particles, improving the composite's performance. The effect of continued recycling of printed PLA/WF parts has yet to be studied and is necessary for establishing the service lifetime or number of times the material can be recycled before being repurposed or disposed of in another way. The feasibility and benefit of mechanical recycling of PLA/WF AM parts was demonstrated in this study in terms of material performance retention and energy savings; additionally, a cost comparison of the virgin and recycled material considering equipment and labor costs would be required to determine the industrial applicability of this work. The effect of recycling on end-of-life considerations such as biodegradability and pyrolysis or solvolysis efficiency is also currently unknown and should be included in future recycling analyses. Finally, as new bio-derived resins and reinforcing fibers, additives, and processing aides become more widely available, the potential for recycling or other valorization processes must be studied to establish sustainable practices for these materials.

Declaration of competing interest

The authors declare that they have no known competing financial interests or personal relationships that could have appeared to influence the work reported in this paper.

Data availability

Data will be made available on request.

Acknowledgements

The authors acknowledge the support from the US Department of Energy (DOE) Advanced Materials and Manufacturing Technologies Office and used resources at the Manufacturing Demonstration Facility at Oak Ridge National Laboratory, a User Facility of DOE's Office of Energy Efficiency and Renewable Energy. This manuscript has been authored by UT-Battelle, LLC under CPS 848 Agreement 35714 with the U.S. Department of Energy. The United States Government retains and the publisher, by accepting the article for publication, acknowledges that the United States Government retains a nonexclusive, paid-up, irrevocable, worldwide license to publish or reproduce the published form of this manuscript, or allow others to do so, for United States Government purposes. The Department of Energy will provide public access to these results of federally sponsored research in accordance with the DOE Public Access Plan (<http://energy.gov/downloads/doe>

-public-access-plan). Microscopy and spectroscopy studies were completed at the Center for Nanophase Materials Sciences, a DOE Office of Science User Facility.

Appendix A. Supplementary data

Supplementary data to this article can be found online at <https://doi.org/10.1016/j.compositesb.2023.110617>.

References

- [1] Lamm ME, et al. Material extrusion additive manufacturing of wood and lignocellulosic filled composites. *Polymers* Sep 17 2020;12(9). <https://doi.org/10.3390/polym12092115>.
- [2] Cerdas F, Juraschek M, Thiede S, Herrmann C. Life cycle assessment of 3D printed products in a distributed manufacturing system. *J Ind Ecol* 2017;21(S1):S80–93. <https://doi.org/10.1111/jiec.12618>.
- [3] Sepasgozar SME, Shi A, Yang L, Shiowzhan S, Edwards DJ. Additive manufacturing applications for industry 4.0: a systematic critical review. *Buildings* 2020;10(12). <https://doi.org/10.3390/buildings10120231>.
- [4] Ajinjeru C, et al. Rheological survey of carbon fiber-reinforced high-temperature thermoplastics for big area additive manufacturing tooling applications. *J Thermoplast Compos* Nov 2019;34(11):1443–61. <https://doi.org/10.1177/0892705719873941> (in English).
- [5] Torrado Perez AR, Roberson DA, Wicker RB. Fracture surface analysis of 3D-printed tensile specimens of novel ABS-based materials. *J Fail Anal Prev* 2014;14(3):343–53. <https://doi.org/10.1007/s11668-014-9803-9>.
- [6] Fuqua MA, Huo S, Ulven CA. Natural fiber reinforced composites. *Polym Rev* 2012;52(3):259–320. <https://doi.org/10.1080/15583724.2012.705409>.
- [7] Storz H, Vorlop K. Bio-based plastics: status, challenges, and trends. *Landbauforschung Völkenrode* 2013;63:321–32. https://doi.org/10.3220/LBF_2013_321-332.
- [8] Gardner DJ, Wang L, Wang J. Additive manufacturing of wood-based materials for composite applications. In: Presented at the 2019 SPE automotive composites conference & exhibition, novi, Michigan, USA; 2019.
- [9] Pilla S, Gong S, O'Neill E, Rowell RM, Krzyzak AM. Polylactide-pine wood flour composites. *Polym Eng Sci Mar* 2008;48(3):578–87. <https://doi.org/10.1002/pen.20971> (in English).
- [10] Zhao X, et al. Recycling of natural fiber composites: challenges and opportunities. *Resour Conserv Recycl* 2022;177. <https://doi.org/10.1016/j.resconrec.2021.105962>.
- [11] Jiang J, Gu H, Li B, Zhang J. Preparation and properties of straw/PLA wood plastic composites for 3D printing. *IOP Conf Ser Earth Environ Sci* 2021;692(3). <https://doi.org/10.1088/1755-1315/692/3/032004>.
- [12] Huang Y, Löschke S, Proust G. In the mix: the effect of wood composition on the 3D printability and mechanical performance of wood-plastic composites. *Composites Part C: Open Access* 2021;5. <https://doi.org/10.1016/j.jcomc.2021.100140>.
- [13] Sloan J. Composites speed concrete facade fabrication [Online]. Available: <https://www.compositesworld.com/articles/composites-speed-concrete-facade-fabrication-5/29/2020>.
- [14] Cruz Sanchez FA, Boudaoud H, Camargo M, Pearce JM. Plastic recycling in additive manufacturing: a systematic literature review and opportunities for the circular economy. *J Clean Prod* 2020;264. <https://doi.org/10.1016/j.jclepro.2020.121602>.
- [15] Shanmugam V, et al. Polymer recycling in additive manufacturing: an opportunity for the circular economy. *Mater. Circular Econ.* 2020;2(1). <https://doi.org/10.1007/s42824-020-00012-0>.
- [16] Bhattacharjee S, Bajwa DS. Feasibility of reprocessing natural fiber filled poly (lactic acid) composites: an in-depth investigation. *Adv Mater Sci Eng* 2017;2017:1–10. <https://doi.org/10.1155/2017/1430892>.
- [17] Morreale M, Liga A, Mistretta MC, Ascione L, Mantia FP. Mechanical, thermomechanical and reprocessing behavior of green composites from biodegradable polymer and wood flour. *Materials* Nov 11 2015;8(11):7536–48. <https://doi.org/10.3390/ma8115406>.
- [18] Alexandre A, Cruz Sanchez FA, Boudaoud H, Camargo M, Pearce JM. Mechanical properties of direct waste printing of polylactic acid with universal pellets extruder: comparison to fused filament fabrication on open-source desktop three-dimensional printers. *3D Print Addit Manuf* 2020;7(5):237–47. <https://doi.org/10.1089/3dp.2019.0195>.
- [19] Woern AL, Byard DJ, Oakley RB, Fiedler MJ, Snabes SL, Pearce JM. Fused particle fabrication 3-D printing: recycled materials' optimization and mechanical properties. *Materials* Aug 12 2018;11(8). <https://doi.org/10.3390/ma11081413>.
- [20] Vidakis N, Petousis M, Maniadis A, Koudoumas E, Vairis A, Kechagias J. Sustainable additive manufacturing: mechanical response of acrylonitrile-butadiene-styrene over multiple recycling processes. *Sustainability* 2020;12(9). <https://doi.org/10.3390/su12093568>.
- [21] Kishore V, Hassen A. Polymer and composites additive manufacturing: material extrusion processes. In: Pou J, Riveiro A, Davim JP, editors. *Additive manufacturing*. Amsterdam, Netherlands: Elsevier; 2021. p. 183–218. *Handbooks in Advanced Manufacturing*, J. P. Davim and K. Gupta, ch. 6.
- [22] Roschli A, et al. Designing for big area additive manufacturing. *Addit Manuf* Jan 2019;25:275–85. <https://doi.org/10.1016/j.addma.2018.11.006> (in English).
- [23] Fischer EW, Sterzel HJ, Wegner G. Investigation of the structure of solution grown crystals of lactide copolymers by means of chemical reactions. *Kolloid-Zeitschrift und Zeitschrift für Polymere* 1973;251:980–90.
- [24] Ruiz EM, Levova T, Reinhard J, Valsasina L, Bourgault G, Werner G. Documentation of changes implemented in the ecoinvent database v3.3, 3.3. Zurich, Switzerland: EcoInvent; 2016.
- [25] Whyman S, Arif KM, Potgieter J. Design and development of an extrusion system for 3D printing biopolymer pellets. *Int J Adv Manuf Technol* 2018;96(9–12):3417–28. <https://doi.org/10.1007/s00170-018-1843-y>.
- [26] Smith T, et al. Dual material system for polymer large scale additive manufacturing. In: Sampe 2020. Seattle, WA: Society for the Advancement of Material and Process Engineering; 2020. May 4–7, 2020, [in Additive Manufacturing].
- [27] Ingeo™ biopolymer 4043D technical data sheet [Online] Available, <https://www.natureworksllc.com/Products/4-series-for-films-cards>.
- [28] Kishore V, et al. Infrared preheating to improve interlayer strength of big area additive manufacturing (BAAM) components. *Addit Manuf* Mar 2017;14:7–12. <https://doi.org/10.1016/j.addma.2016.11.008> (in English).
- [29] Levenhagen NP, Dadmun MD. Improving interlayer adhesion in 3D printing with surface segregating additives: improving the isotropy of acrylonitrile-butadiene-styrene parts. *ACS Appl. Poly. Mater.* 2019;1(4):876–84. <https://doi.org/10.1021/acspnm.9b00051>.
- [30] Duty C, Failla J, Kim S, Smith T, Lindahl J, Kunc V. Z-Pinning approach for 3D printing mechanically isotropic materials. *Addit Manuf* 2019;27:175–84. <https://doi.org/10.1016/j.addma.2019.03.007>.
- [31] Torrado AR, Shemelya CM, English JD, Lin Y, Wicker RB, Roberson DA. Characterizing the effect of additives to ABS on the mechanical property anisotropy of specimens fabricated by material extrusion 3D printing. *Addit Manuf* 2015;6:16–29. <https://doi.org/10.1016/j.addma.2015.02.001>.
- [32] Levenhagen NP, Dadmun MD. Reactive processing in extrusion-based 3D printing to improve isotropy and mechanical properties. *Macromolecules* 2019;52(17):6495–501. <https://doi.org/10.1021/acs.macromol.9b01178>.
- [33] Levenhagen NP, Dadmun MD. Interlayer diffusion of surface segregating additives to improve the isotropy of fused deposition modeling products. *Polymer* 2018;152:35–41. <https://doi.org/10.1016/j.polymer.2018.01.031>.
- [34] Spreeman ME, Stretz HA, Dadmun MD. Role of compatibilizer in 3D printing of polymer blends. *Addit Manuf* 2019;27:267–77. <https://doi.org/10.1016/j.addma.2019.03.009>.
- [35] Ngo TD, Kashani A, Imbalzano G, Nguyen KTQ, Hui D. Additive manufacturing (3D printing): a review of materials, methods, applications and challenges. *Compos B Eng* 2018;143:172–96. <https://doi.org/10.1016/j.compositesb.2018.02.012>.
- [36] Petchwattana N, Nakpan N, Narupai B. A circular economy use of waste wood sawdust for wood plastic composite production: effect of bio-plasticiser on the toughness. *Int J Sustain Eng* Sep 2 2020;13(5):398–410. <https://doi.org/10.1080/19397038.2019.1688422> (in English).
- [37] Tokdemir V, Altun S. A case study of wood thermoplastic composite filament for 3D printing. *Bioresources* 2021;17(1):21–36. <https://doi.org/10.15376/biores.17.1.21-36>.
- [38] Beltran FR, Lorenzo V, Acosta J, de la Orden MU, Martinez Urreaga J. Effect of simulated mechanical recycling processes on the structure and properties of poly (lactic acid). *J Environ Manag* Jun 15 2018;216:25–31. <https://doi.org/10.1016/j.jenvman.2017.05.020>.
- [39] Ngaothong C, et al. Recycling of sisal fiber reinforced polypropylene and polylactic acid composites: thermo-mechanical properties, morphology, and water absorption behavior. *Waste Manag* Sep 2019;97:71–81. <https://doi.org/10.1016/j.wasman.2019.07.038>.
- [40] Åkesson D, Vrignaud T, Tissot C, Skrifvars M. Mechanical recycling of PLA filled with a high level of cellulose fibres. *J Polym Environ* 2016;24(3):185–95. <https://doi.org/10.1007/s10924-016-0760-0>.
- [41] Chaitanya S, Singh I, Song JI. Recyclability analysis of PLA/Sisal fiber biocomposites. *Compos B Eng* 2019;173. <https://doi.org/10.1016/j.compositesb.2019.05.106>.
- [42] Shahi P, Behravesh AH, Daryabaray SY, Lotfi M. Experimental investigation on reprocessing of extruded wood flour/HDPE composites. *Polym Compos* 2012;33(5):753–63. <https://doi.org/10.1002/pc.22201>.
- [43] Wang L, Sanders JE, Gardner DJ, Han Y. Effect of fused deposition modeling process parameters on the mechanical properties of a filled polypropylene. *Prog Add Manufact* 2018;3(4):205–14. <https://doi.org/10.1007/s40964-018-0053-3>.
- [44] Tekinalp HL, et al. Highly oriented carbon fiber-polymer composites via additive manufacturing. *Compos Sci Technol* Dec 10 2014;105:144–50. <https://doi.org/10.1016/j.compscitech.2014.10.009> (in English).
- [45] Penumakala PK, Santo J, Thomas A. A critical review on the fused deposition modeling of thermoplastic polymer composites. *Compos B Eng* 2020;201. <https://doi.org/10.1016/j.compositesb.2020.108336>.
- [46] Saeed K, et al. Characterization of continuous carbon fibre reinforced 3D printed polymer composites with varying fibre volume fractions. *Compos Struct* 2022;282. <https://doi.org/10.1016/j.compstruct.2021.115033>.
- [47] Komal UK, Lila MK, Singh I. PLA/banana fiber based sustainable biocomposites: a manufacturing perspective. *Compos B Eng* 2020;180. <https://doi.org/10.1016/j.compositesb.2019.107535>.
- [48] Yang D, Zhang H, Wu J, McCarthy ED. Fibre flow and void formation in 3D printing of short-fibre reinforced thermoplastic composites: an experimental benchmark exercise. *Addit Manuf* 2021;37. <https://doi.org/10.1016/j.addma.2020.101686>.
- [49] Mattingly F, Franc A, Kunc V, Duty C. Characterizing internal porosity of 3D-printed fiber reinforced materials. In: International solid freeform fabrication

- symposium. Austin, TX, USA: University of Texas at Austin; 2021. <https://doi.org/10.26153/tsw/17578>.
- [50] Duty CE, et al. Structure and mechanical behavior of big area additive manufacturing (BAAM) materials. *Rapid Prototyp J* 2017;23(1):181–9. <https://doi.org/10.1108/Rpj-12-2015-0183> (in English).
- [51] Montalvo Navarrete JI, Hidalgo-Salazar MA, Escobar Nunez E, Rojas Arciniegas AJ. Thermal and mechanical behavior of biocomposites using additive manufacturing. *Int J Interact Des Manuf* 2017;12(2):449–58. <https://doi.org/10.1007/s12008-017-0411-2>.
- [52] Martins G, Antunes F, Mateus A, Malca C. Optimization of a wood plastic composite for architectural applications. *Procedia Manuf* 2017;12:203–20. <https://doi.org/10.1016/j.promfg.2017.08.025> (in English).
- [53] Li M, et al. Recent advancements of plant-based natural fiber-reinforced composites and their applications. *Compos B Eng* 2020;200. <https://doi.org/10.1016/j.compositesb.2020.108254>.
- [54] Beltrán FR, Infante C, de la Orden MU, Martínez Urreaga J. Mechanical recycling of poly(lactic acid): evaluation of a chain extender and a peroxide as additives for upgrading the recycled plastic. *J Clean Prod* 2019;219:46–56. <https://doi.org/10.1016/j.jclepro.2019.01.206>.
- [55] Mahi H, Rodrigue D. Linear and non-linear viscoelastic properties of ethylene vinyl acetate/nano-crystalline cellulose composites. *Rheol Acta* 2011;51(2):127–42. <https://doi.org/10.1007/s00397-011-0603-9>.
- [56] Kashi S, Gupta RK, Baum T, Kao N, Bhattacharya SN. Phase transition and anomalous rheological behaviour of polylactide/graphene nanocomposites. *Compos B Eng* 2018;135:25–34. <https://doi.org/10.1016/j.compositesb.2017.10.002>.
- [57] Jubinville D, Esmizadeh E, Tzoganakis C, Mekonnen T. Thermo-mechanical recycling of polypropylene for the facile and scalable fabrication of highly loaded wood plastic composites. *Compos B Eng* 2021;219. <https://doi.org/10.1016/j.compositesb.2021.108873>.
- [58] Letwimolnun W, Vergnes B, Ausias G, Carreau PJ. Stress overshoots of organoclay nanocomposites in transient shear flow. *J Non-Newtonian Fluid Mech* 2007;141(2–3):167–79. <https://doi.org/10.1016/j.jnnfm.2006.11.003>.
- [59] Copenhaver K, et al. Recycled cardboard containers as a low energy source for cellulose nanofibrils and their use in poly(l-lactide) nanocomposites. *ACS Sustainable Chem Eng* 2021;9(40):13460–70. <https://doi.org/10.1021/acssuschemeng.1c03890>.
- [60] Adam G, Hay J, Parsons I, Haward R. Effect of molecular weight on the thermal properties of polycarbonates. *Polymer* 1976;17:51–7.
- [61] Lu SX, Cebe P. Thermal analysis study of the effect of molecular weight on constrained amorphous phase in poly(phenylene sulfide). *J Therm Anal* 1997;49(1):525–33. <https://doi.org/10.1007/Bf01987480> (in English).
- [62] Du M, et al. Crystal-nuclei formation during injection-molding of poly (l-lactic acid). *Polymer* 2022;250. <https://doi.org/10.1016/j.polymer.2022.124897>.
- [63] De Santis F, Volpe V, Pantani R. Effect of molding conditions on crystallization kinetics and mechanical properties of poly(lactic acid). *Polym Eng Sci* 2017;57(3):306–11. <https://doi.org/10.1002/pen.24414>.
- [64] Compton BG, Post BK, Duty CE, Love L, Kunz V. Thermal analysis of additive manufacturing of large-scale thermoplastic polymer composites. *Addit Manuf* Oct 2017;17:77–86. <https://doi.org/10.1016/j.addma.2017.07.006> (in English).
- [65] Spoerl M, Sapkota J, Weingrill G, Fischinger T, Arbeiter F, Holzer C. Shrinkage and warpage optimization of expanded-perlite-filled polypropylene composites in extrusion-based additive manufacturing. *Macromol Mater Eng* 2017;302(10). <https://doi.org/10.1002/mame.201700143>.